Molecular Cell
Article

# Structural Basis for Translational Stalling by Human Cytomegalovirus and Fungal Arginine Attenuator Peptide

Shashi Bhushan,[1,5] Helge Meyer,[2,3] Agata L. Starosta,[1] Thomas Becker,[1] Thorsten Mielke,[4] Otto Berninghausen,[1] Michael Sattler,[2,3] Daniel N. Wilson,[1,*] and Roland Beckmann[1,*]

[1]Gene Center and Department of Biochemistry and Center for integrated Protein Science Munich, University of Munich, Feodor-Lynen-Strasse 25, 81377 Munich, Germany

[2]Institute of Structural Biology, Helmholtz Zentrum München, Ingolstädter Landstrasse 1, 85764 Neuherberg, Germany

[3]Munich Center for Integrated Protein Science at Department Chemie, Technische Universität München, Lichtenbergstrasse 4, 85747 Garching, Germany

[4]Institut für Medizinische Physik und Biophysik, Charité, Ziegelstrasse 5-8, 10117 Berlin, Germany

[5]Present address: Rudolf Virchow Center, DFG Research Center for Experimental Biomedicine, Josef-Schneider-Strasse 2, 97080 Würzburg, Germany

*Correspondence: wilson@lmb.uni-muenchen.de (D.N.W.), beckmann@lmb.uni-muenchen.de (R.B.)

DOI 10.1016/j.molcel.2010.09.009

## SUMMARY

**Specific regulatory nascent chains establish direct interactions with the ribosomal tunnel, leading to translational stalling. Despite a wealth of biochemical data, structural insight into the mechanism of translational stalling in eukaryotes is still lacking. Here we use cryo-electron microscopy to visualize eukaryotic ribosomes stalled during the translation of two diverse regulatory peptides: the fungal arginine attenuator peptide (AAP) and the human cytomegalovirus (hCMV) gp48 upstream open reading frame 2 (uORF2). The C terminus of the AAP appears to be compacted adjacent to the peptidyl transferase center (PTC). Both nascent chains interact with ribosomal proteins L4 and L17 at tunnel constriction in a distinct fashion. Significant changes at the PTC were observed: the eukaryotic-specific loop of ribosomal protein L10e establishes direct contact with the CCA end of the peptidyl-tRNA (P-tRNA), which may be critical for silencing of the PTC during translational stalling. Our findings provide direct structural insight into two distinct eukaryotic stalling processes.**

## INTRODUCTION

The ribosomal exit tunnel is an ~90–100 Å long conduit, located in the large ribosomal subunit, through which the nascent chain passes as it is being synthesized. It has long been assumed that the tunnel is inert with respect to the nascent chains; however, growing evidence indicates an important role for the exit tunnel in protein folding (Bhushan et al., 2010; Hardesty and Kramer, 2001; Lu and Deutsch, 2005; Tu and Deutsch, 2010; Woolhead et al., 2004) and translation regulation (Lovett, 1994; Morris and Geballe, 2000; Tenson and Ehrenberg, 2002). Indeed, a wide variety of regulated bacterial operons have been discovered where ribosome stalling during translation of a short upstream open reading frame (uORF), or so-called leader peptide, regulates expression of the downstream cistron. Well-characterized examples include the SecM (secretion monitor) (Nakatogawa and Ito, 2002; Yap and Bernstein, 2009), ErmCL (erythromycin resistance) (Ramu et al., 2009), and TnaC (tryptophanase) (Gong and Yanofsky, 2002) leader peptides. A recent cryo-EM structure of a TnaC-stalled ribosome revealed direct interaction between the TnaC peptide and the ribosomal tunnel (Seidelt et al., 2009); however, no evidence for a cascade of conformational ribosomal RNA (rRNA) rearrangements, as previously proposed for SecM stalling (Mitra et al., 2006), was observed.

Similarly, regulatory peptides operate in eukaryotes, the most well-studied being the fungal AAP and the hCMV glycoprotein (gp48) uORFs (Morris and Geballe, 2000). During an early stage of CMV infection, the expression of gp48 is repressed by the CMV uORF2 (Degnin et al., 1993; Geballe et al., 1986). Translation of the CMV uORF2 peptide inhibits termination at its own stop codon, thereby blocking scanning to the downstream initiation codon of gp48 (Degnin et al., 1993; Geballe et al., 1986). The CMV-stalled ribosome contains a Pro-tRNA at the P site and a stop codon at the A site, both of which are critical for stalling (Cao and Geballe, 1996; Janzen et al., 2002). In contrast, translational stalling by the AAP requires an additional *trans*-acting effector molecule, namely the amino acid L-arginine (Arg) (Wang and Sachs, 1997a; Wang and Sachs, 1997b). In the presence of high concentrations of Arg, stalling during translation of the AAP uORF leads to downregulation of carbamoyl phosphate synthetase A in *N. crassa* and *S. cerevisiae*. Like CMV, stalling of AAP occurs naturally at a stop codon; however, unlike CMV, a stop codon is not a prerequisite for stalling (Fang et al., 2000; Wang et al., 1998). Thus, AAP exhibits antitermination as well as antielongation properties, distinguishing it from CMV. Nevertheless, mutation of specific residues of both the CMV (Alderete et al., 1999; Degnin et al., 1993) and AAP

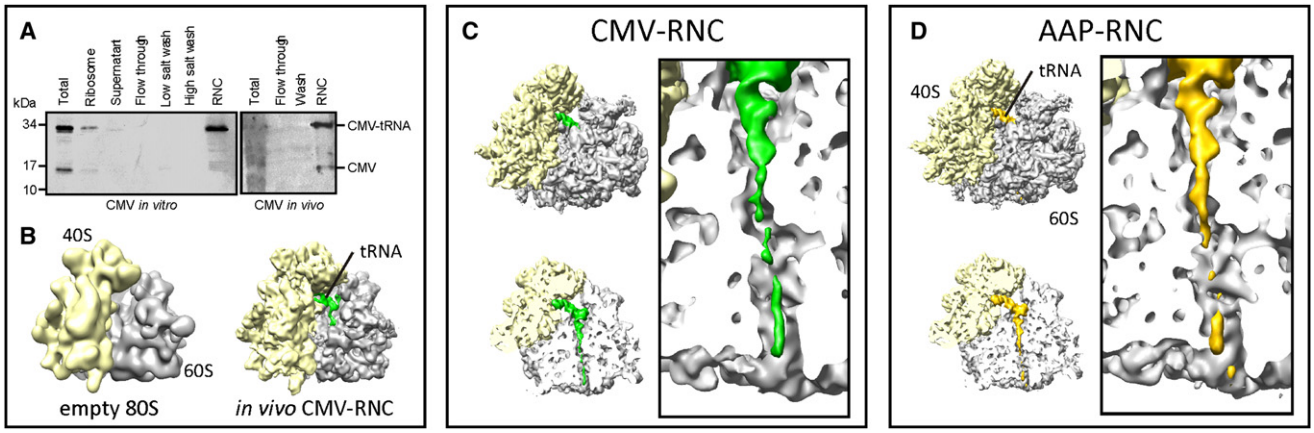


**Figure 1. Preparation and Cryo-EM Reconstructions of AAP- and CMV-RNCs**

(A) Purification of in vitro-stalled wheat germ CMV-RNCs and in vivo-stalled endogenous yeast CMV-RNCs. SDS-PAGE and western blot analysis of the in vitro and in vivo RNC preparations. Indicated fractions (1% of total, 0.5% of pelleted ribosome, 1% of supernatant and flowthrough, 5% of low- and high-salt wash, and 5% of purified RNCs) were applied on to a 15% SDS-PAGE gel, transferred to a PVDF membrane, and detected using primary anti-HA antibody and secondary HRP-coupled antibody.

(B–D) (B) Reconstructions of yeast 80S ribosome control and the in vivo yeast CMV-RNC. Cryo-EM reconstruction of the in vitro (C) AAP- and (D) CMV-RNCs, at 6.5 Å and 6.7 Å resolution, respectively (see Figure S1), with overview (top left), transverse section (bottom left), and zoom of ribosomal tunnel (right-hand boxed inset). Sec61 is not shown, whereas the 40S subunit is colored light yellow, 60S is gray, and AAP and CMV peptidyl-tRNAs are gold and green, respectively.

(Delbecq et al., 2000; Freitag et al., 1996; Wang and Sachs, 1997b) has been shown to abolish the regulatory effect of these peptides, suggesting that a direct interaction of the stalling peptides with components of the tunnel is critical for stalling. Despite this wealth of biochemical data (Morris and Geballe, 2000), direct structural insight into the mechanism of translational stalling in eukaryotes is still lacking.

Here we have used cryo-EM and single-particle reconstruction to determine structures of eukaryotic ribosomes stalled during the translation of the fungal AAP uORF and the human CMV gp48 uORF2. The C terminus of the AAP appears to be compacted adjacent to the peptidyl transferase center (PTC), consistent with NMR data demonstrating the high α-helical propensity of this region. At the tunnel constriction, both the CMV and AAP nascent chains appear to be stabilized, where they interact in a distinct fashion with ribosomal proteins L4 and L17. Moreover, we observe differences at the PTC, namely for the loop of eukaryotic-specific ribosomal protein L10e as well as in the vicinity of nucleotide A2602 (*E. coli* numbering). Specifically, the loop of ribosomal protein L10e establishes direct contact with the CCA end of the peptidyl-tRNA (P-tRNA), which may be critical for silencing of the PTC during translational stalling. Collectively, these findings provide direct structural insight into two distinct eukaryotic stalling processes.

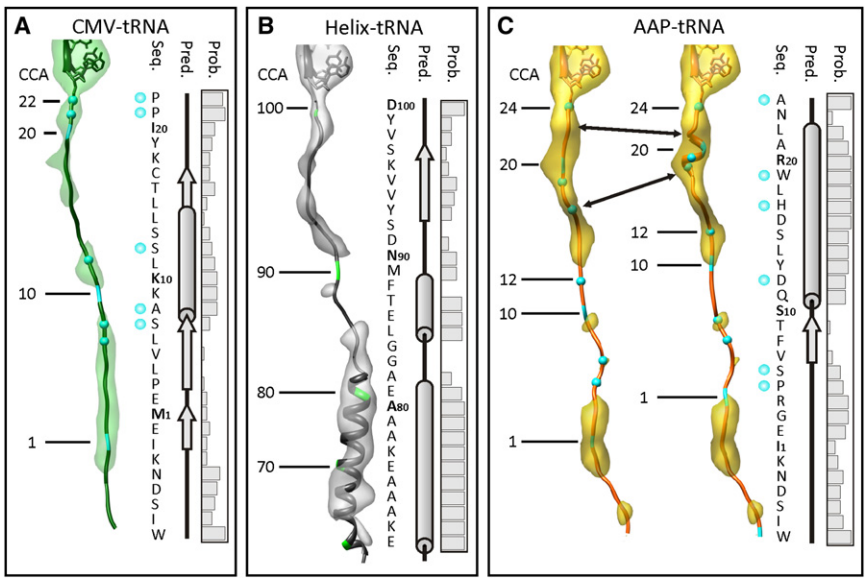


**Figure 2. Molecular Models of the AAP and CMV Peptide**

Isolated density with fitted models for (A) CMV-tRNA, (B) Helix-tRNA (Bhushan et al., 2010), and (C) AAP-tRNA. The sequence (Seq.) of each peptide is given with secondary structure prediction (Pred.) and probability (Prob.) determined using PSIPRED. The cyan balls indicate residues that abolish stalling when mutated.

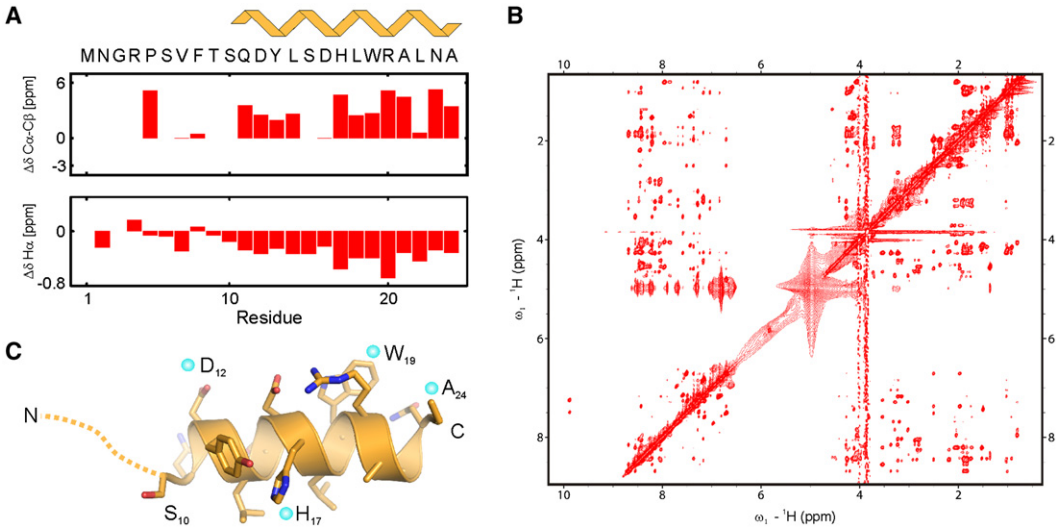


**Figure 3. Nuclear Magnetic Resonance Spectroscopy of the AAP**

(A) Secondary chemical shifts of the AAP in 50% (v/v) TFE.

(B) NOESY spectrum of 1 mM AAP in 50% (v/v) TFE recorded with a mixing time of 100 ms at 900 MHz and a temperature of 277 K (see also Figure S2).

(C) Ribbon representation of the NMR structure encompassing residues 9–24.

## RESULTS AND DISCUSSION

### Generation and Visualization of Eukaryotic AAP- and CMV-Stalled RNCs

To gain direct structural insight into the eukaryotic stalling mechanism, CMV- and AAP-stalled RNCs were generated using a *Triticum aestivum* (wheat germ) in vitro translation system (see the Experimental Procedures). In both cases, we observed stalling activity and detected the presence of P-tRNA in the purified RNCs, further corroborating the efficient translational stalling. This is consistent with the finding that the AAP retains regulatory function in plant and animal cell-free systems (Fang et al., 2004). Similarly, we found that the hCMV peptide could efficiently stall translation in wheat germ (Figure 1A), rabbit reticulocyte lysate (Cao and Geballe, 1996), fruitfly, and yeast translation extracts (data not shown). We were also able to overexpress the CMV uORF in growing yeast and isolate the endogenously stalled CMV-RNCs (Figure 1A). A cryo-EM structure of the in vivo CMV-RNCs clearly showed the presence of P-tRNA (Figure 1B), indicating the potential use of the in vivo-generated CMV-RNCs for structural and biochemical studies. Single-particle analysis of the in vitro-stalled CMV- and AAP-RNCs resulted in highly resolved density maps (Figures 1C and 1D) at 6.5 Å and 6.7 Å resolution, respectively (see Figure S1 available online). In both structures, we observed strong density for a tRNA in the P site, linked to the nascent chain (Figures 1C and 1D).

### Molecular Models for the AAP and CMV Nascent Chains

The densities for the P-tRNAs were isolated, fitted with molecular models, and compared with our recent structure of eukaryotic Helix-RNC (Bhushan et al., 2010) (Figures 2A–2C). The density for the CMV nascent chain is consistent with an extended conformation in the tunnel (Figure 2A). In this extended model, residues of the CMV peptide that are critical for translation regulation (Alderete et al., 1999; Cao and Geballe, 1996) are positioned in density (Figure 2A), suggesting that these regions are stabilized within the tunnel. In contrast, a large region of significantly stronger density was observed for the C-terminal region of the AAP (Figure 2C), suggesting some compaction of the nascent chain within this region. Curiously, secondary structure predictions indicate that the C-terminal region of the AAP (specifically residues 11–21) has a high propensity to adopt an α-helical conformation (Figure 2C) (Hood et al., 2007), analogous to the distal region of the nascent peptide observed in the Helix-RNC (Bhushan et al., 2010) (Figure 2B). Therefore, we generated two models for the AAP, one extended and a second where a turn of an α helix was introduced to indicate compaction in this region of the peptide (Figure 2C). In this alternative model, compaction of the peptide relocates Asp12 into density, which is in agreement with data demonstrating the importance of this residue for stalling (Freitag et al., 1996). Moreover, the mutations His18Pro and Trp20Pro in the C-terminal region of *S. cerevisae* AAP (His17 and Trp19 in *N. crassa*), which would preclude helix formation, also abolish translation regulation (Delbecq et al., 2000). The repositioning of critical residues by compaction of the distal region of the AAP nascent chain is reminiscent of the influence that neighboring residues have on the placement of Arg163 during SecM-mediated translation stalling (Yap and Bernstein, 2009).

### CD and NMR Spectroscopic Analysis Reveal the Helical Propensity of the AAP

In order to investigate the helical propensity of the AAP, the entire peptide was synthesized and analyzed by circular dichroism (CD). The CD spectrum indicates typical characteristics for

**Table 1. Structure Statistics for NMR of AAP**

| | |
|---|---|
| Distance Restraints | |
| Intraresidual, sequential[a] | 167 |
| Medium range (two to four)[a] | 79 |
| Long range (five or more)[a] | 0 |
| H bond restraints[a] | 18 |
| Total[a] | 264 |
| Torsion Angle Restraints | |
| $\Phi + \psi$ dihedral angle restraints[b] | 22 |
| Coordinate Precision Rmsd | |
| Backbone (Å) | 0.28 ± 0.1 |
| Heavy atom (Å) | 0.82 ± 0.14 |
| Consistency (Structure versus Restraints) | |
| Rmsd (Å) from experimental distance restraints[1] | 0.015 ± 0.002 |
| Rmsd (°) from experimental torsion angle restraints[b] | 0.492 ± 0.160 |
| Ramachandran Plot | |
| Most favored regions[c] | 96.9 % |
| Allowed regions[c] | 3.1 % |
| Generously allowed regions[c] | 0.0 % |
| Disallowed regions[c] | 0.0 % |

Statistics are given for the 20 lowest energy structures after water refinement out of 100 calculated. The CNS $E_{repel}$ function was used to simulate van der Waals interactions with an energy constant of 25 kcal mol$^{-1}$ Å$^{-4}$ using "PROLSQ" van der Waals radii. RMSD and PROCHECK values apply for residues 10–24.

[a] Distance restraints were employed with a soft square-well potential using an energy constant of 50 kcal mol$^{-1}$ Å$^{-2}$. No distance restraint was violated by more than 0.5 Å.

[b] Torsion angle restraints derived from TALOS were applied to $\phi$, $\psi$ backbone angles using energy constants of 200 kcal mol$^{-1}$ rad$^{-2}$. No dihedral angle restraint was violated by more than 5°.

[c] PROCHECK was used to determine the quality of the structure.

random coil; however, in the presence of 50% (v/v) trifluoroethanol (TFE), helix formation was observed (Figure S2). It is known that helicity within regions of peptides with intrinsic helical propensity is promoted by this organic cosolvent (Lehrman et al., 1990). Subsequently, we used nuclear magnetic resonance (NMR) spectroscopy in 50% (v/v) TFE solution to identify the regions of the peptide containing helical elements. As shown in Figure 3A, the secondary chemical shifts indicate that the C terminus can indeed adopt an α-helical conformation, whereas the N-terminal region appears to be disordered. Homonuclear $^1$H NOESY experiments (Figure 3B and Figure S3) were combined with dihedral angle restraints derived from secondary chemical shifts to determine the structure of the helical region of the AAP (Figure 3C and Table 1). It should be noted that the low α-helical stability of peptide fragments with known helical structure in the native protein is a common observation and results mainly from the absence of stabilizing long-range intramolecular interactions that are present in the folded protein (Lehrman et al., 1990). This implies that the ribosomal tunnel provides a specific environment that promotes the observed helical or compacted structure of the AAP. Computer simulations, for example, suggest that confinement in roughly cylindrical tubes, analogous to the ribosomal tunnel, entropically stabilizes α helix formation (O'Brien et al., 2008; Ziv et al., 2005).

## Stabilization of Nascent Peptides within Distinct Regions of the Ribosomal Tunnel

Docking of a molecular model of the ribosomal tunnel (Bhushan et al., 2010) into the CMV- and AAP-RNC maps allowed us to identify the sites of interaction between the nascent peptides and the tunnel (Figures 4A and 4B). Notably, there is a good correlation between the suggested interaction pattern derived from our maps and previous mutagenesis studies, such that mutation of nascent peptide residues involved in strong interactions abolish translational stalling, whereas mutations with minor effects on stalling affect residues forming no or only weak interactions (a complete list of mutations known to effect stalling of AAP and CMV is included in Table 2): in the upper part of the tunnel, strong density is seen connecting the C-terminal residues of AAP and CMV with the 28S rRNA in the region of nucleotides U2585 (*E. coli* numbering is used throughout) and A2062. Replacing the terminal Ala24 with a stop codon in AAP (Wang and Sachs, 1997b) and mutation of either Pro21 or Pro22 (to Ala) in CMV (Degnin et al., 1993) abolishes translational stalling. At lower thresholds, additional contacts are observed from both nascent chains toward the positions of U2609 and A2058. In bacterial stalling systems, such as ErmC and TnaC, mutations of U2609, A2062, and in the U2585 region have been shown to abolish translational regulation (Cruz-Vera et al., 2005; Vazquez-Laslop et al., 2008; Yang et al., 2009).

At the constriction where the extensions of ribosomal proteins L17 and L4 converge, the AAP and CMV nascent chains interact with the tunnel in a distinct manner: the density for the CMV peptide in this region suggests that it is stabilized around residues 10–12 (Figure 4A), with Ser12 indeed being essential for stalling. Notably, density is not observed in this region even when a nascent chain with high helical propensity is positioned there (Bhushan et al., 2010). Apparently, interactions of the CMV peptide with the β-hairpin of L17, the A751 region, and the distal extension of L4 are responsible for this stabilization. AAP forms a similar contact around residues 11–12, which are sandwiched between L17/A751 on one side of the tunnel and the proximal extension of L4 on the other. An additional contact, however, is also observed between the region around residues 6–7 and the distal extension of L4 (Figure 4B). The residues of the AAP and CMV nascent chains that are stabilized at the constriction are highly conserved, and mutation of these residues (indicated by cyan spheres in Figures 2–4) abolishes translational stalling in both systems (Alderete et al., 1999; Delbecq et al., 2000; Freitag et al., 1996; Hood et al., 2007). Furthermore, mutations in the β-hairpin of L22 (the bacterial homolog of L17) as well as insertions at A751 relieve the translational arrest in the bacterial SecM and/or TnaC stalling systems (Cruz-Vera et al., 2005; Nakatogawa and Ito, 2002). This suggests that the constriction plays a universal role in translational stalling, but also that the identity of the interaction can be distinct for each nascent chain. Additionally, it should be noted that stabilization of the CMV and AAP nascent chains is also observed toward the N terminus (Figures 2A and 2C), in a similar region where helix formation was suggested by biochemical experiments (Lu and Deutsch,

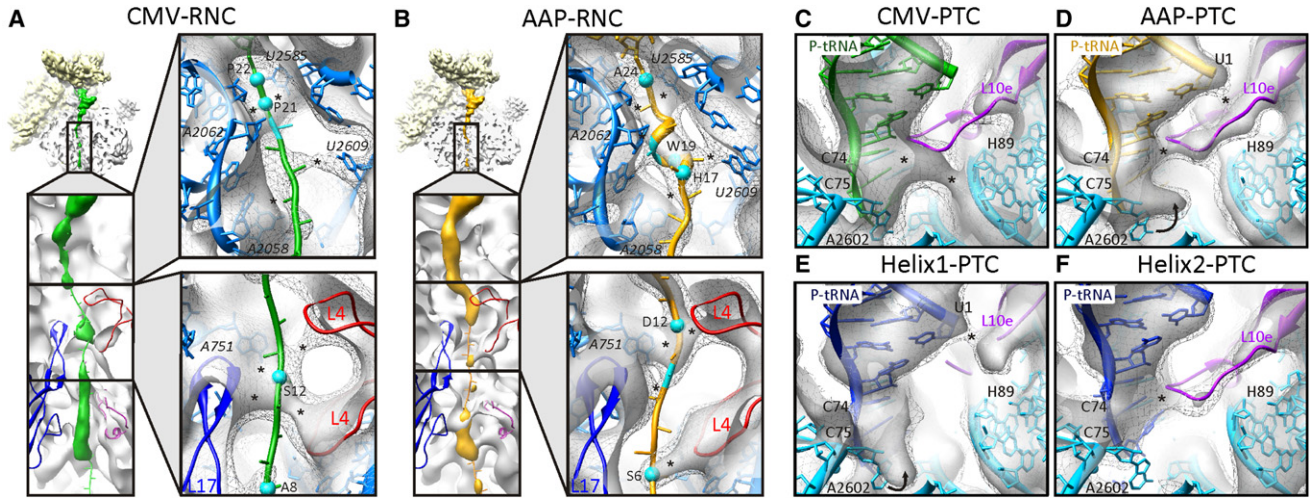


**Figure 4. Contacts between the AAP and CMV Nascent Chains and the Ribosomal Tunnel**

(A and B) Transverse sections of the large ribosomal subunit of the (A) CMV- and (B) AAP-RNCs to reveal the sites of interaction between the nascent chains and components of the ribosomal tunnel. In the enlarged panels of the upper and middle tunnel regions, the density is shown at two thresholds (with the lower threshold in mesh). CMV (green) and AAP (gold) nascent chains are shown as ribbons with cyan balls indicating critical residues of for translational stalling. Asterisks indicate sites of contact between the nascent chains and ribosomal components. Residues in the nascent chain are labeled as single-letter amino acids (as in Figure 2), whereas the nucleotides of 28S rRNA are labeled using italics. L4 and L17 refer to ribosomal proteins L4 and L17.

(C–F) Comparison of the PTC of (C) CMV- and (D) AAP-stalling peptidyl-tRNAs, with nonstalling (E) Helix1- and (F) Helix2-RNCs (Bhushan et al., 2010) (see also Figure S3). rRNA is colored cyan and L10e is magenta. Asterisks indicate sites of contact between L10e and P-tRNA or rRNA. The cryo-EM density is shown at two thresholds (with the lower threshold in mesh). In (D) and (E), the arrow indicates a possible shift in the position of A2602 in the AAP- and Helix1-RNCs.

2005; Tu and Deutsch, 2010) and observed previously by cryo-EM (Figure 2B) (Bhushan et al., 2010). This may be relevant for CMV stalling, since mutation of Ser7 or Ala8 significantly reduces translation regulation (Alderete et al., 1999). In contrast, deletion or mutation of the first four residues of AAP has no effect on translational stalling (Delbecq et al., 2000).

**Table 2. Contacts between CMV and AAP Nascent Chains and the Ribosomal Tunnel**

| CMV Residue | Ribosomal Contact Partner | Ribosomal Component | Mutagenesis Data/Reference |
|---|---|---|---|
| **Pro22**[a] | U2585/A2062[a] | 28S rRNA[b] | Abolishes stalling (Alderete et al., 1999; Degnin et al., 1993) |
| **Pro21** | U2585/A2062 | 28S rRNA | Abolishes stalling (Degnin et al., 1993) |
| (Ile20-Tyr19)[c] | A2062 | 28S rRNA | Minor effect (Degnin et al., 1993) |
| (Lys18)[3] | U2609 | 28S rRNA | Minor effect (Degnin et al., 1993) |
| (Cys17-Thr16)[c] | A2058/2059 | | Minor effect (Alderete et al., 1999) |
| **Ser12** | A751 | 28S rRNA | Abolishes stalling (Degnin et al., 1993) |
| **Ser12**/(Leu11)[c] | Gly86-Thr88/ Arg136-Asn138 | L4/ L17 | Abolishes stalling (Degnin et al., 1993) |
| (Ala7-**Ser8**)[c] | Tyr37-Asn38 | L39e | Abolishes stalling (Alderete et al., 1999) |
| AAP Residue | Ribosomal Contact Partner | Ribosomal Component | Mutagenesis Data/Reference |
| **Ala24**-Asn23[a] | U2585/A2062[b] | 28S rRNA | Abolishes stalling (Delbecq et al., 2000; Wang and Sachs, 1997b) |
| Arg20 | A2062 | 28S rRNA | Minor effect (Delbecq et al., 2000) |
| (**Trp19**-**His17**)[c] | U2609 | 28S rRNA | Abolishes stalling (Delbecq et al., 2000) |
| (**Asp16**-Leu14)[c] | A2058/2059 | 28S rRNA | Abolishes stalling (Delbecq et al., 2000) |
| **Asp12**-Gln11 | A751 | 28S rRNA | Abolishes stalling (Delbecq et al., 2000; Freitag et al., 1996) |
| **Asp12**-Gln11 | Gly74-Val77 | L4 | Abolishes stalling (Delbecq et al., 2000; Freitag et al., 1996) |
| (Ser10-**Thr9**)*[c] | Arg136-Asn138 | L17 | Diverse effects (Delbecq et al., 2000) |
| **Ser6** | Thr88-Arg90 | L4 | Abolishes stalling (Delbecq et al., 2000) |

[a] Positions are approximate so the closest residue(s) to the contact site is given based on fitting of CMV and AAP nascent chain and ribosome structures to the cryo-EM density.

[b] Numbering is given using *E. coli* for rRNA, rice (*O. sativa*) for L4 and L17, and wheat germ (*T. aestivum*) for L39e.

[c] Density corresponding to these interactions was only observed at low thresholds, suggesting weak interactions.

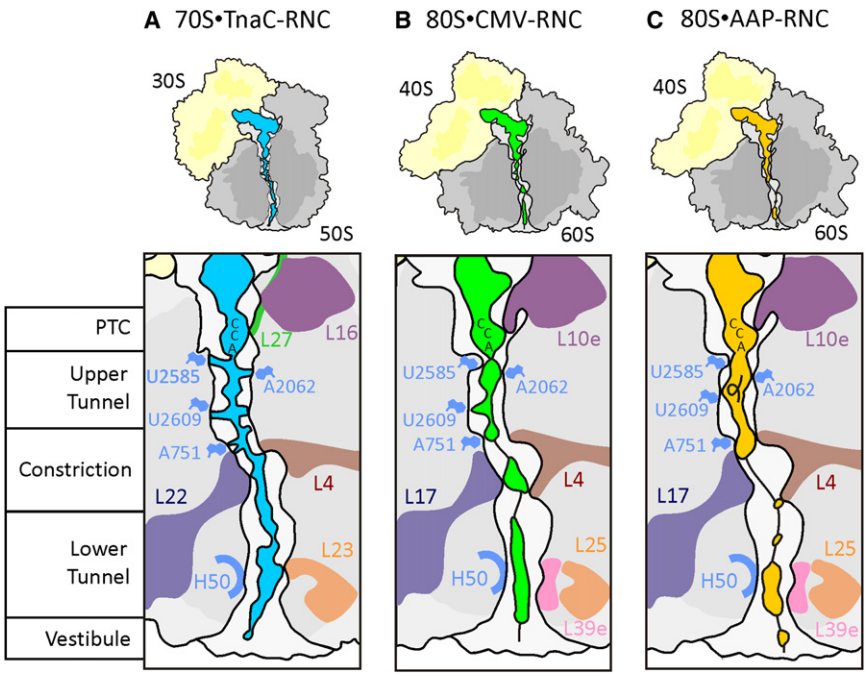


**Figure 5. Comparison of Bacterial and Eukaryotic Translational Stalling**

Schematic view of (A) the bacterial TnaC•70S-RNC, with the eukaryotic (B) CMV- and (C) AAP-RNCs with overview (above) and zoom on ribosomal tunnel (below).

## Conformational Changes at the Peptidyl Transferase Center

Comparison of the positions of the CCA ends of the CMV-/AAP-tRNAs with nonstalling helix1/2-tRNAs does not reveal any significant differences at this resolution (Figure 5 and Figure S4). However, one clear difference at the PTC of the AAP- and CMV-RNCs is seen in the vicinity of A2602. This base is highly flexible and observed in different conformations depending on the functional state of the ribosome (Seidelt et al., 2009). Consistent with this flexibility, we observe very weak density in the region of A2602 in the CMV-RNC (Figure 4C); however, in the AAP-RNC, strong density is seen directly adjacent to the CCA end of the P-tRNA that could accommodate a specific orientation of the base (Figure 4D). A distinct conformation for A2602, incompatible with release factor action, was also observed in the PTC of the TnaC-stalled ribosome (Seidelt et al., 2009), which by analogy may suggest that the conformation of A2602 in the AAP-RNC is important for the antitermination mechanism of AAP.

Notably, strong density for the loop of ribosomal protein L10e is observed at the PTC contacting the CCA end of the AAP-tRNA (Figure 4D). There is also density connecting the CCA end of the CMV-tRNA with the backbone of H89, which we attribute to stabilization of the tip of the loop of L10e (Figure 4C). In the crystal structure of the archaeal large subunit (Ban et al., 2000), the loop of L10e was disordered and not modeled, suggesting that it is highly flexible. This is consistent with the weak or lacking density of this loop in our previous Helix-RNCs (Figures 4E and 4F) (Bhushan et al., 2010). Thus, it is tempting to speculate that the loop of L10e has a general role in tRNA positioning, consistent with mutations and deletions in this loop being lethal (Hofer et al., 2007), and a specific role in translational stalling.

## Conclusion

Structurally, the PTC and ribosomal tunnel are highly conserved between bacteria and eukaryotes. The major differences are in the ribosomal proteins L4, the distal loop of which is much longer in eukaryotes, the presence of L38e at the tunnel exit, and the loop of L10e at the PTC (Figure 5). Comparison of the bacterial TnaC-stalled RNC (Seidelt et al., 2009) (Figure 5A) with the eukaryotic CMV- and AAP-stalled RNCs (Figures 5B and 5C) reveals a number of general features. First, there is no cascade of conformational rearrangements, as proposed for SecM stalling (Mitra et al., 2006). Second, interactions of the nascent chains are established with a discrete set of tunnel components, such as rRNA nucleotides U2585, A2062, A2058, A751, and the extensions of L4 and L17 (L22) (Figure 5). We note that it may not be the interaction per se that is important for stalling, but rather that certain residues may play a role in positioning of neighboring critical residues, as observed for SecM stalling (Yap and Bernstein, 2009). Third, stabilization of the nascent chain is evident within the tunnel constriction (Figure 5), in a region where density has not been observed for nonregulatory peptides (Bhushan et al., 2010). Additionally, each stalling mechanism employs distinct features that are specific for the nascent peptide. For example, L10e, the loop of which is absent in bacteria, may play a role in AAP stalling by tRNA positioning and/or stabilization. Conformational change in the region of A2602 may play a role in the AAP and TnaC antitermination mechanisms, whereas CMV may function differently. At this resolution, it is not possible to determine the origin of the conformational changes at the PTC, but they may be relayed from the nascent chain either through the chain itself or through subtle conformational changes in components of the ribosome, as suggested previously for TnaC stalling (Seidelt et al., 2009). Additionally, compaction is observed in the fungal AAP stalling RNC adjacent to the PTC, while the conformation of the human CMV and bacterial TnaC-stalling peptides are essentially extended (Figure 5). Taken together, despite the high degree of conservation of the ribosomal tunnel, no apparent consensus emerges for the stalling peptide interactions. To the contrary, apart from a general involvement of the tunnel constriction, evolutionary diverse stalling sequences, from bacteria, fungi, and viruses, appear to employ distinct mechanisms to induce translational regulation.

## EXPERIMENTAL PROCEDURES

### Stalling Construct and In Vitro RNC Preparation

The CMV and AAP constructs were generated using a T7 standard forward primer with either a modified reverse cmv (5′-TTAAGGAGGAATATATTTGC AGGTCAGCAGGCTGCTCAGTTTTTTCGCACTCAGCACCAGCGGTTCCATT TCAATTTTATTGTCACTAATCCATT-3′) or reverse aap (5′-TTACGCGTTAAG GGCTCTCCACAGATGGTCTGAGAGGTAATTCTGACTAGTGAA GACTGACG GGCGACCTTCAATTTTATTGTCACTAATCCATT-3′) primer, using the DPAP-B120 (without signal anchor sequence) construct as a template (Halic et al., 2004). Uncapped transcripts were then synthesized from the PCR fragments using T7 RNA polymerase. Both the CMV- and AAP-RNCs were generated using a homemade wheat germ in vitro translation system (based on Erickson and Blobel [1983]) programmed with mRNA encoding the DPAPB-CMV and DPAPB-AAP fusion proteins. RNCs were purified as described previously (Halic et al., 2004).

### Generation of Endogenously Stalled In Vivo RNCs

The CMV stalling construct was cloned in to a yeast expression pYES2.1 TOPO vector (Invitrogen) under galactose-inducible GAL1 promoter. Yeast cells were transformed with the pYES2.1 vector, and positive transformed cells were selected using the URA marker. Cells were grown overnight in 50 ml of SC-U minimal media containing 2% glucose at 30°C. Overnight grown cells were pelleted and resuspended in 1 L of induction media (SC-U supplemented with 2% galactose) to have a final $OD_{600}$ of 0.4. Growth was continued at 30°C and cells harvested at an $OD_{600}$ of 2.0. Cell pellets were stored in −80°C until needed, or dissolved in buffer A (50 mM Tris-Cl [pH 7.0], 250 mM potassium acetate, 25 mM magnesium acetate, 10 μg/ml cyclohexamide, 5 mM β-mercaptoethanol, 250 mM sucrose, 0.1% [w/v] Nikkol, 0.1% [w/v] protease inhibitor [1 pill/ml], 0.2 U/ml RNase inhibitor). Cells were broken with a microfluidizer and the lysate was cleared by spinning at 20,000 × g for 15 min at 4°C. The cleared lysate was then incubated with Talon resin (Clontech) for 15 min at 4°C, and the resin was washed ten times with buffer A. Resin-bound RNCs were eluted using buffer A containing 100 mM imidazole. The eluted RNCs were then concentrated by centrifugation through a sucrose cushion (50 mM Tris-HCl [pH 7.0], 500 mM potassium acetate, 25 mM magnesium acetate, 10 μg/ml cyclohexamide, 5 mM β-mercaptoethanol, 1 M sucrose, 0.1% [w/v] Nikkol, 0.1% [w/v] protease inhibitor [pill/ml], 0.2 U/ml RNase inhibitor) at 100,000 rpm in a bench top Beckmann ultra centrifuge in TLA 110 rotor. Pelleted RNCs were dissolved in buffer B (50 mM Tris-HCl [pH 7.0], 50 mM potassium acetate, 2.5 mM magnesium acetate, 100 μg/ml cyclohexamide, 5 mM DTT, 125 mM sucrose, 0.05% [w/v] Nikkol, 0.5% [w/v] protease inhibitor [1 pill/ml], 0.2 U/ml RNase inhibitor). RNCs were aliquoted in small volumes, flash frozen in liquid nitrogen, and then stored at −80°C. A small data set (30,000 particles) of in vivo-stalled CMV-RNCs were recorded and processed as described below for the in vitro-prepared RNCs.

### Electron Microscopy, Image Processing, and Modeling

As described previously (Wagenknecht et al., 1988), samples were applied to carbon-coated holey grids. To avoid orientational bias, the wheat germ RNCs were reconstituted with a 5-fold molar excess of Sec61 as described (Becker et al., 2009). Micrographs were then recorded under low-dose conditions (25 electrons/$Å^2$) with a magnification of 38,900 on a Tecnai F30 field emission gun electron microscope at 300 kV in a defocus range of 1.0–4.5 μm. Micrographs were scanned on a Heidelberg Primescan D8200 drum scanner, resulting in a pixel size of 1.24 Å on the object scale. The data were analyzed by determination of the contrast transfer function using CTFFIND (Mindell and Grigorieff, 2003). The data were further processed with the SPIDER software package (Frank et al., 1996). After automated particle picking followed by visual inspection, 180,000 particles for CMV-RNCs and 200,000 particles for AAP-RNC were selected for density reconstruction. Both the data sets were sorted into programmed (with P-tRNA) and unprogrammed/empty (without P-tRNA) ribosome sub-data sets, using reconstructions of programmed and unprogrammed ribosomes as references. Removal of unprogrammed ribosome particles resulted in 150,000 and 165,000 programmed particles for CMV-RNC and AAP-RNC, respectively. This yielded final CTF-corrected reconstructions at a resolution of 6.5 Å and 6.7 Å, respectively, based on the Fourier shell correlation (FSC) with a cut-off value of 0.5 (Figure S1). Densities for the 40S subunit, the 60S subunit and the P site tRNA were isolated using binary masks. Models were generated as described previously (Bhushan et al., 2010). Models were generated using an extended version of MANIP (Massire and Westhof, 1998) and then refined and fitted using RNAVIEW (Yang et al., 2003) and MDFF (Trabuco et al., 2008). Protein alignments were built with TCoffee (Notredame et al., 2000). Homology models for ribosomal proteins were built using Modeler (Eswar et al., 2006). Models were then adjusted manually with Coot (Emsley and Cowtan, 2004) and minimized with VMD (Humphrey et al., 1996). The CCA-Pro and CCA-Ala positions of the nascent chains were modeled based on an alignment with the *Haloarcula marismortui* 50S subunit in complex with CCA-pcb (Schmeing et al., 2005a, 2005b). Initial docking of X-ray structures and models was performed using Chimera (Pettersen et al., 2004), and alignment of pdbs was performed using PyMol (http://www.pymol.org/). All figures were generated using Chimera (Pettersen et al., 2004).

### Circular Dichroism Spectroscopy

Far-UV (190–250 nm) CD spectra were recorded on 30 μM AAP in 20 mM $PO_4^-$, 25 mM sodium chloride and 0% (v/v) or 50% (v/v) TFE using a JASCO J-715 spectropolarimeter (Figure S2). The sample temperature for all CD measurements was maintained at 293 K.

### Nuclear Magnetic Resonance Spectroscopy

NMR measurements were carried out on a Bruker Avance III 750 MHz spectrometer equipped with a TXI probehead, and on an Avance 900 instrument equipped with a TXI cryoprobehead, respectively. NOESY (mixing times of 100 and 300 ms) (Jeener et al., 1979), TOCSY (Bax and Davis, 1985; Müller and Ernst, 1979) (mixing times of 100 ms), and $^1H$, $^{13}C$ HSQC (Kay et al., 1992; Palmer et al., 1991; Schleucher et al., 1994; Willker et al., 1993) spectra were recorded on 1 mM AAP in 20 mM phosphate buffer, with 50 mM sodium chloride at pH 6.5, and 0% (v/v) or 50% (v/v) TFE, respectively (Figure 3 and Figure S3). Spectra were recorded at 277 or 298 K. NMR spectra were processed with NMRPipe (Delaglio et al., 1995) and analyzed with Sparky (http://www.cgl.ucsf.edu/home/sparky/). Automated NOE cross-peak assignment was performed using the software CYANA 2.1 (Guntert, 2009). Automatically assigned NOEs and the completeness of the NOE cross-peaks were manually checked. Distance restraints from the CYANA calculation and TALOS+ (Shen et al., 2009)-derived torsion angles restraints were used for refinement in a box of water molecules (Linge et al., 2003) using Aria 2.2 (Rieping et al., 2007). Statistics are given in Table 1 for the 20 lowest energy structures (see Figure S3) after water refinement out of 100 calculated. The CNS $E^{repel}$ function was used to simulate van der Waals interactions with an energy constant of 25 kcal $mol^{-1}$ $Å^{-4}$ using "PROLSQ" van der Waals radii. Quality of the structure ensemble was validated using the program PROCHECK (Laskowski et al., 1996).

## ACCESSION NUMBERS

The cryo-electron microscopic maps of the AAP-RNC and CMV-RNC have been deposited in the 3D-EM database under accession numbers EMD-1767 and EMD-1768, respectively, and the NMR structure of the AAP in the Protein Data Bank under ID code 2XL1.

## SUPPLEMENTAL INFORMATION

Supplemental Information includes three figures and can be found with this article at doi:10.1016/j.molcel.2010.09.009.

## ACKNOWLEDGMENTS

We would like to thank Carol Deutsch for critical reading of the manuscript and J. Buerger for help with the electron microscopy. This research was supported by a Knut och Alice Wallenbergs Stiftelse postdoctoral fellowship (to S.B.), grants from the Deutsche Forschungsgemeinschaft SFB594 and SFB646 (to

R.B.), SFB740 (to T.M.), and WI3285/1-1 (to D.N.W.) and by the European Union and Senatsverwaltung für Wissenschaft, Forschung und Kultur Berlin.

Received: April 7, 2010
Revised: May 28, 2010
Accepted: July 30, 2010
Published: October 7, 2010

## REFERENCES

Alderete, J.P., Jarrahian, S., and Geballe, A.P. (1999). Translational effects of mutations and polymorphisms in a repressive upstream open reading frame of the human cytomegalovirus UL4 gene. J. Virol. *73*, 8330–8337.

Ban, N., Nissen, P., Hansen, J., Moore, P.B., and Steitz, T.A. (2000). The complete atomic structure of the large ribosomal subunit at 2.4 Å resolution. Science *289*, 905–920.

Bax, A., and Davis, D.G. (1985). Mlev-17-based two-dimensional homonuclear magnetization transfer spectroscopy. J. Magn. Reson. *65*, 355–360.

Becker, T., Bhushan, S., Jarasch, A., Armache, J.P., Funes, S., Jossinet, F., Gumbart, J., Mielke, T., Berninghausen, O., Schulten, K., et al. (2009). Structure of monomeric yeast and mammalian Sec61 complexes interacting with the translating ribosome. Science *326*, 1369–1373.

Bhushan, S., Gartmann, M., Halic, M., Armache, J.P., Jarasch, A., Mielke, T., Berninghausen, O., Wilson, D.N., and Beckmann, R. (2010). α-helical nascent polypeptide chains visualized within distinct regions of the ribosomal exit tunnel. Nat. Struct. Mol. Biol. *17*, 313–317.

Cao, J.H., and Geballe, A.P. (1996). Inhibition of nascent-peptide release at translation termination. Mol. Cell. Biol. *16*, 7109–7114.

Cruz-Vera, L., Rajagopal, S., Squires, C., and Yanofsky, C. (2005). Features of ribosome-peptidyl-tRNA interactions essential for tryptophan induction of tna operon expression. Mol. Cell *19*, 333–343.

Degnin, C.R., Schleiss, M.R., Cao, J., and Geballe, A.P. (1993). Translational inhibition mediated by a short upstream open reading frame in the human cytomegalovirus gpUL4 (gp48) transcript. J. Virol. *67*, 5514–5521.

Delaglio, F., Grzesiek, S., Vuister, G.W., Zhu, G., Pfeifer, J., and Bax, A. (1995). NMRPipe: a multidimensional spectral processing system based on UNIX pipes. J. Biomol. NMR *6*, 277–293.

Delbecq, P., Calvo, O., Filipkowski, R.K., Pierard, A., and Messenguy, F. (2000). Functional analysis of the leader peptide of the yeast gene CPA1 and heterologous regulation by other fungal peptides. Curr. Genet. *38*, 105–112.

Emsley, P., and Cowtan, K. (2004). Coot: model-building tools for molecular graphics. Acta Crystallogr. D Biol. Crystallogr. *60*, 2126–2132.

Erickson, A.H., and Blobel, G. (1983). Cell-free translation of messenger RNA in a wheat germ system. Methods Enzymol. *96*, 38–50.

Eswar, N., Webb, B., Marti-Renom, M.A., Madhusudhan, M.S., Eramian, D., Shen, M.Y., Pieper, U., and Sali, A. (2006). Comparative protein structure modeling using Modeller. Curr. Protoc. Bioinformatics, *Chapter 5*, Unit 5.6.

Fang, P., Wang, Z., and Sachs, M.S. (2000). Evolutionarily conserved features of the arginine attenuator peptide provide the necessary requirements for its function in translational regulation. J. Biol. Chem. *275*, 26710–26719.

Fang, P., Spevak, C., Wu, C., and Sachs, M. (2004). A nascent polypeptide domain that can regulate translation elongation. Proc. Natl. Acad. Sci. USA *101*, 4059–4064.

Frank, J., Radermacher, M., Penczek, P., Zhu, J., Li, Y., Ladjadj, M., and Leith, A. (1996). SPIDER and WEB: processing and visualization of images in 3D electron microscopy and related fields. J. Struct. Biol. *116*, 190–199.

Freitag, M., Dighde, N., and Sachs, M.S. (1996). A UV-induced mutation in neurospora that affects translational regulation in response to arginine. Genetics *142*, 117–127.

Geballe, A.P., Spaete, R.R., and Mocarski, E.S. (1986). A cis-acting element within the 5′ leader of a cytomegalovirus beta transcript determines kinetic class. Cell *46*, 865–872.

Gong, F., and Yanofsky, C. (2002). Instruction of translating ribosome by nascent peptide. Science *297*, 1864–1867.

Guntert, P. (2009). Automated structure determination from NMR spectra. Eur. Biophys. J. *38*, 129–143.

Halic, M., Becker, T., Pool, M., Spahn, C., Grassucci, R., Frank, J., and Beckmann, R. (2004). Structure of the signal recognition particle interacting with the elongation-arrested ribosome. Nature *427*, 808–814.

Hardesty, B., and Kramer, G. (2001). Folding of a nascent peptide on the ribosome. Prog. Nucleic Acid Res. Mol. Biol. *66*, 41–66.

Hofer, A., Bussiere, C., and Johnson, A.W. (2007). Mutational analysis of the ribosomal protein Rpl10 from yeast. J. Biol. Chem. *282*, 32630–32639.

Hood, H.M., Spevak, C.C., and Sachs, M.S. (2007). Evolutionary changes in the fungal carbamoyl-phosphate synthetase small subunit gene and its associated upstream open reading frame. Fungal Genet. Biol. *44*, 93–104.

Humphrey, W., Dalke, A., and Schulten, K. (1996). VMD—visual molecular dynamics. J. Mol. Graph. *14*, 33–38.

Janzen, D.M., Frolova, L., and Geballe, A.P. (2002). Inhibition of translation termination mediated by an interaction of eukaryotic release factor 1 with a nascent peptidyl-tRNA. Mol. Cell. Biol. *22*, 8562–8570.

Jeener, J., Meier, B.H., Bachmann, P., and Ernst, R.R. (1979). Investigation of exchange processes by 2-dimensional NMR-spectroscopy. J. Chem. Phys. *71*, 4546–4553.

Kay, L.E., Keifer, P., and Saarinen, T. (1992). Pure absorption gradient enhanced heteronuclear single quantum correlation spectroscopy with improved sensitivity. J. Am. Chem. Soc. *114*, 10663–10665.

Laskowski, R.A., Rullmannn, J.A., MacArthur, M.W., Kaptein, R., and Thornton, J.M. (1996). AQUA and PROCHECK-NMR: programs for checking the quality of protein structures solved by NMR. J. Biomol. NMR *8*, 477–486.

Lehrman, S.R., Tuls, J.L., and Lund, M. (1990). Peptide alpha-helicity in aqueous trifluoroethanol: correlations with predicted alpha-helicity and the secondary structure of the corresponding regions of bovine growth hormone. Biochemistry *29*, 5590–5596.

Linge, J.P., Williams, M.A., Spronk, C.A., Bonvin, A.M., and Nilges, M. (2003). Refinement of protein structures in explicit solvent. Proteins *50*, 496–506.

Lovett, P.S. (1994). Nascent peptide regulation of translation. J. Bacteriol. *176*, 6415–6417.

Lu, J., and Deutsch, C. (2005). Folding zones inside the ribosomal exit tunnel. Nat. Struct. Mol. Biol. *12*, 1123–1129.

Massire, C., and Westhof, E. (1998). MANIP: an interactive tool for modelling RNA. J. Mol. Graph. Model. *16*, 197–205, 255–197.

Mindell, J.A., and Grigorieff, N. (2003). Accurate determination of local defocus and specimen tilt in electron microscopy. J. Struct. Biol. *142*, 334–347.

Mitra, K., Schaffitzel, C., Fabiola, F., Chapman, M.S., Ban, N., and Frank, J. (2006). Elongation arrest by SecM via a cascade of ribosomal RNA rearrangements. Mol. Cell *22*, 533–543.

Morris, D.R., and Geballe, A.P. (2000). Upstream open reading frames as regulators of mRNA translation. Mol. Cell. Biol. *20*, 8635–8642.

Müller, L., and Ernst, R.R. (1979). Coherence transfer in the rotating frame—application to heteronuclear cross-correlation spectroscopy. Mol. Phys. *38*, 963–992.

Nakatogawa, H., and Ito, K. (2002). The ribosomal exit tunnel functions as a discriminating gate. Cell *108*, 629–636.

Notredame, C., Higgins, D.G., and Heringa, J. (2000). T-Coffee: a novel method for fast and accurate multiple sequence alignment. J. Mol. Biol. *302*, 205–217.

O'Brien, E.P., Stan, G., Thirumalai, D., and Brooks, B.R. (2008). Factors governing helix formation in peptides confined to carbon nanotubes. Nano Lett. *8*, 3702–3708.

Palmer, A.G., III, Cavanagh, J., Wright, P.E., and Rance, M. (1991). Sensitivity improvement in Proton-detected 2-dimensional heteronuclear correlation NMR-spectroscopy. J. Magn. Reson. *93*, 151–170.

Pettersen, E.F., Goddard, T.D., Huang, C.C., Couch, G.S., Greenblatt, D.M., Meng, E.C., and Ferrin, T.E. (2004). UCSF Chimera—a visualization system for exploratory research and analysis. J. Comput. Chem. *25*, 1605–1612.

Ramu, H., Mankin, A., and Vazquez-Laslop, N. (2009). Programmed drug-dependent ribosome stalling. Mol. Microbiol. *71*, 811–824.

Rieping, W., Habeck, M., Bardiaux, B., Bernard, A., Malliavin, T.E., and Nilges, M. (2007). ARIA2: automated NOE assignment and data integration in NMR structure calculation. Bioinformatics *23*, 381–382.

Schleucher, J., Schwendinger, M., Sattler, M., Schmidt, P., Schedletzky, O., Glaser, S.J., Sorensen, O.W., and Griesinger, C. (1994). A general enhancement scheme in heteronuclear multidimensional NMR employing pulsed field gradients. J. Biomol. NMR *4*, 301–306.

Schmeing, T.M., Huang, K.S., Kitchen, D.E., Strobel, S.A., and Steitz, T.A. (2005a). Structural insights into the roles of water and the 2′ hydroxyl of the P site tRNA in the peptidyl transferase reaction. Mol. Cell *20*, 437–448.

Schmeing, T.M., Huang, K.S., Strobel, S.A., and Steitz, T.A. (2005b). An induced-fit mechanism to promote peptide bond formation and exclude hydrolysis of peptidyl-tRNA. Nature *438*, 520–524.

Seidelt, B., Innis, C.A., Wilson, D.N., Gartmann, M., Armache, J.P., Villa, E., Trabuco, L.G., Becker, T., Mielke, T., Schulten, K., et al. (2009). Structural insight into nascent polypeptide chain-mediated translational stalling. Science *326*, 1412–1415.

Shen, Y., Delaglio, F., Cornilescu, G., and Bax, A. (2009). TALOS+: a hybrid method for predicting protein backbone torsion angles from NMR chemical shifts. J. Biomol. NMR *44*, 213–223.

Tenson, T., and Ehrenberg, M. (2002). Regulatory nascent peptides in the ribosomal tunnel. Cell *108*, 591–594.

Trabuco, L.G., Villa, E., Mitra, K., Frank, J., and Schulten, K. (2008). Flexible fitting of atomic structures into electron microscopy maps using molecular dynamics. Structure *16*, 673–683.

Tu, L.W., and Deutsch, C. (2010). A folding zone in the ribosomal exit tunnel for Kv1.3 helix formation. J. Mol. Biol. *396*, 1346–1360.

Vazquez-Laslop, N., Thum, C., and Mankin, A.S. (2008). Molecular mechanism of drug-dependent ribosome stalling. Mol. Cell *30*, 190–202.

Wagenknecht, T., Frank, J., Boublik, M., Nurse, K., and Ofengand, J. (1988). Direct localization of the tRNA-anticodon interaction site on the Escherichia coli 30 S ribosomal subunit by electron microscopy and computerized image averaging. J. Mol. Biol. *203*, 753–760.

Wang, Z., and Sachs, M.S. (1997a). Arginine-specific regulation mediated by the Neurospora crassa arg-2 upstream open reading frame in a homologous, cell-free in vitro translation system. J. Biol. Chem. *272*, 255–261.

Wang, Z., and Sachs, M.S. (1997b). Ribosome stalling is responsible for arginine-specific translational attenuation in Neurospora crassa. Mol. Cell. Biol. *17*, 4904–4913.

Wang, Z., Fang, P., and Sachs, M.S. (1998). The evolutionarily conserved eukaryotic arginine attenuator peptide regulates the movement of ribosomes that have translated it. Mol. Cell. Biol. *18*, 7528–7536.

Willker, W., Leibfritz, D., Kerssebaum, R., and Bermel, W. (1993). Gradient selection in inverse heteronuclear correlation spectroscopy. Magn. Reson. Chem. *31*, 287–292.

Woolhead, C.A., McCormick, P.J., and Johnson, A.E. (2004). Nascent membrane and secretory proteins differ in FRET-detected folding far inside the ribosome and in their exposure to ribosomal proteins. Cell *116*, 725–736.

Yang, H., Jossinet, F., Leontis, N., Chen, L., Westbrook, J., Berman, H., and Westhof, E. (2003). Tools for the automatic identification and classification of RNA base pairs. Nucleic Acids Res. *31*, 3450–3460.

Yang, R., Cruz-Vera, L.R., and Yanofsky, C. (2009). 23S rRNA nucleotides in the peptidyl transferase center are essential for tryptophanase operon induction. J. Bacteriol. *191*, 3445–3450.

Yap, M.N., and Bernstein, H.D. (2009). The plasticity of a translation arrest motif yields insights into nascent polypeptide recognition inside the ribosome tunnel. Mol. Cell *34*, 201–211.

Ziv, G., Haran, G., and Thirumalai, D. (2005). Ribosome exit tunnel can entropically stabilize alpha-helices. Proc. Natl. Acad. Sci. USA *102*, 18956–18961.